ISCI, Volume *22*

Supplemental Information

Voltage Does Not Drive Prestin (SLC26a5) Electro-Mechanical Activity at High Frequencies Where Cochlear Amplification Is Best

Joseph Santos-Sacchi and Winston Tan

Transparent Methods

OHCs were isolated from guinea pig and mouse as described previously (Santos-Sacchi et al., 2019; Santos-Sacchi and Tan, 2018). Briefly, animals were killed by anesthetic overdose, the cochleas removed and the organ of Corti of the top two coils dissected out. Following 5 minutes of enzymatic digestion with trypsin (0.5mg/ml), the OHCs were isolated by gentle trituration and placed in a petri dish on a Nikon Eclipse TI-2000 microscope for recording. Extracellular solution was (in mM): NaCl 100, TEA-Cl 20, CsCl 20, $CoCl_2$ 2, $MgCl_2$ 1, $CaCl_2$ 1, Hepes 10, pH 7.2. Extracellular solution was in the patch pipette. Macro-patches on the OHC lateral membrane were made near the middle of the cylindrical cell; since prestin density/activity is uniform within the lateral membrane (Dallos et al., 1991; Huang and Santos-Sacchi, 1993), they provide representative information. For the guinea pig on-cell macro-patch approach we used pipette inner diameters of 3.38 +/- 0.20 μm (electrode resistance in bath 1.46 +/- 0.06 MΩ, n=13), with M-coat applied within about 20 μm of the tip to minimize pipette capacitance. Hemispheric estimate of patch surface area was 179 fF. Mouse pipette tip size was smaller at 2.29 +/- 0.024 μm (n=3). In order to establish Gohm seals (5.54 +/- 0.59 GΩ, n=13) we supplemented extracellular solution with 5-7.5 μM Gd^{+3}; we have shown previously that theses low concentrations help to form seals without affecting NLC (Santos-Sacchi and Song, 2016; Santos-Sacchi et al., 2019). **Fig. 1A-D** illustrates our protocol to measure high frequency NLC. Voltage steps from -160 mV to 160 mV were superimposed with an array of voltage chirps. We have previously shown that breakdown of prestin expressing membrane occurs at voltages greater than 300 mV (Navarrete and Santos-Sacchi, 2006). Nevertheless, patches where instabilities of the membrane produced erratic currents at the largest potentials were removed from our data set. An Axon 200B amplifier was used with jClamp software (www.scisoftco.com). An Axon Digidata 1440 was used for digitizing at 10 μs (Nyquist frequency of 50 kHz). Currents were filtered at 10 kHz with a 4-pole Bessel filter. The voltage chirps were generated in the software program jClamp (www.scisoftco.com) using the Matlab logarithmic "chirp" function (10 mV pk; pts=4096; F0=24.4141 Hz; F1=50 kHz; t1=0.04095 s). Subtraction of currents at very depolarized potentials (160 mV) where NLC is absent (Santos-Sacchi and Navarrete, 2002), provided prestin-associated nonlinear currents, absent stray capacitive currents. Subsequently, these subtracted nonlinear membrane currents were used

for dual-sine or single-sine based capacitance estimation by evaluating real and imaginary components of the differential input admittance (Y_{diff}) derived from the subtracted currents (Santos-Sacchi, 2004; Santos-Sacchi et al., 1998). The removal of stray capacitance is required for the application of membrane capacitance algorithms (see below). Briefly, real and imaginary components of the nonlinear membrane admittance at all chirp frequencies were determined by FFT in jClamp, and corrected for the roll-off of recording system admittance (Gillis, 1995). That is, the frequency response of the system, including all components (AD/DA, amplifier and filter) was assessed by placing a small shielded resistor, 10 MΩ, into the head stage input. Stray capacitance was balanced out with amplifier circuitry prior to grounding the resistor. Then, following grounding, voltage chirps (frequency span from 3.05 to 50 kHz, 32768 points at 10 μs clock) were delivered, and currents recorded to provide system admittance. The magnitude and phase of our system response is shown in **Figure S1 A and B**. That system admittance is used to correct experimental data admittance. The necessity for such corrections are shown in **Figure S1 C-D**, where an electrical cell model (Rs: 10 MΩ, Rm: 2 GΩ, and Cm: 1 pF) was analyzed similar to macro-patches, after stray capacitance compensation with amplifier circuitry. It can be seen, for both the dual sine and single sine analysis, that uncorrected responses are aberrant, but following correction for system magnitude and phase (i.e., dividing the complex response admittance by system admittance at each stimulus frequency), the subsequently estimated capacitance is flat at about 1 pF across frequency, regardless of holding potential. Thus, our methodology permits us to measure capacitance with high fidelity out to 20 kHz across holding potentials. We and others have previously used such an approach, though at lower interrogating frequencies, to measure NLC, as well as capacitance associated with synaptic vesicle release (Santos-Sacchi, 2018; Schnee et al., 2011b; Schnee et al., 2011a; Santos-Sacchi et al., 1998).

For the dual sine method, the solution of the standard electrode-cell model is obtained from the admittances at 2 interrogating frequencies (Santos-Sacchi et al., 1998; Santos-Sacchi, 2018), based on the original single sine solution of Pusch and Neher (Pusch and Neher, 1988). The component solutions at harmonic angular frequencies ω_n, where n=0, 1 and $\omega_n=2\pi f_n$, are

$$R_{s_n} = \frac{a_n - \beta}{{a_n}^2 + {b_n}^2 - a_n \beta}$$

$$R_{m_n} = \frac{1}{b}\frac{((a_n - \beta)^2 + {b_n}^2)}{({a_n}^2 + {b_n}^2 - a_n\beta)}$$

$$C_{m_n} = \frac{1}{(\omega_n b_n)}\frac{\left({a_n}^2 + {b_n}^2 - a_n\beta\right)^2}{((a_n - \beta)^2 + {b_n}^2)}$$

where from the measured input admittance Y_{in} we obtain

$$Y_{cell_{\omega_n}} = Y_{in_{\omega_n}} - Y_{stray_{\omega_n}}, n = 0,1$$

$$a_n = Re\left(Y_{cell_{\omega_n}}\right)$$

$$b_n = Im\left(Y_{cell_{\omega_n}}\right)$$

$$c_n = {a_n}^2 + {b_n}^2$$

$$\beta = -0.5 \times \frac{-c_1 + c_0 + \sqrt{{c_1}^2 - 2\,c_1\,c_0 + {c_0}^2 - 4\,a_1 a_0\,c_1 + 4{a_1}^2\,c_0 + 4\,{a_0}^2\,c_1 - 4\,a_0 a_1\,c_0}}{a_1 - a_0}$$

Thus, membrane currents evoked by two voltage frequencies can be used to solve for R_s, R_m and C_m, even in the face of resistive changes, *but only in the absence of stray capacitance*. This applies to measures of patch capacitance, as well. We report on C_m measures derived from f_n, where n=0.

For single sine analysis, capacitance was estimated from the imaginary component of the admittance, $C_m = Im(Y_{diff})/\omega$, where $\omega = 2\pi f$, after minimizing the real component of admittance by rotating the phase angle of the complex admittance. Single and dual sine frequency response estimates were essentially the same (for example, see **Figure S1 D and F**).

To extract NLC at each frequency, we fit V_m-C_m data to the following *eq. 1* (Santos-Sacchi and Navarrete, 2002). This equation extracts NLC based on a 2-state charge movement (Boltzmann) model, which predicts symmetrical NLC on either side of V_h. In fact, measured membrane capacitance in OHCs or prestin-expressing heterologous cells is greater at hyperpolarized potentials than at depolarized potentials. This voltage-dependent sigmoidal offset is removed by the fit (see **Fig. 1H**). The equation has been routinely used to evaluate NLC (Santos-Sacchi and Song, 2014; Homma and Dallos, 2011; Duret et al., 2017; Chessum et al., 2018; Harasztosi and Gummer, 2016).

eq. 1

$$C_m = Q_{max}\,\frac{ze}{kT}\,\frac{b}{(1+b)^2} + \frac{\Delta C_{sa}}{(1+b^{-1})} + C_0$$

where

$$b = exp\left(\frac{-ze(V_m - V_h)}{kT}\right)$$

Q_{max} is the maximum nonlinear charge moved, V_h is voltage at peak capacitance or equivalently, at half maximum charge transfer, V_m is membrane potential, z is valence, e is electron charge, k is Boltzmann's constant, and T is absolute temperature. C_0 is defined as the capacitance of the membrane when all motors are in their compact state, the minimum membrane capacitance; ΔC_{sa} is the maximum increase in capacitance that occurs when all motors change from compact to expanded state, each motor contributing a unit response of δC_{sa}.

Data are presented as mean +/- standard error (SE). Data points from previous publications were extracted from plots using the application Grabit (written by Jiro Doke) in Matlab.

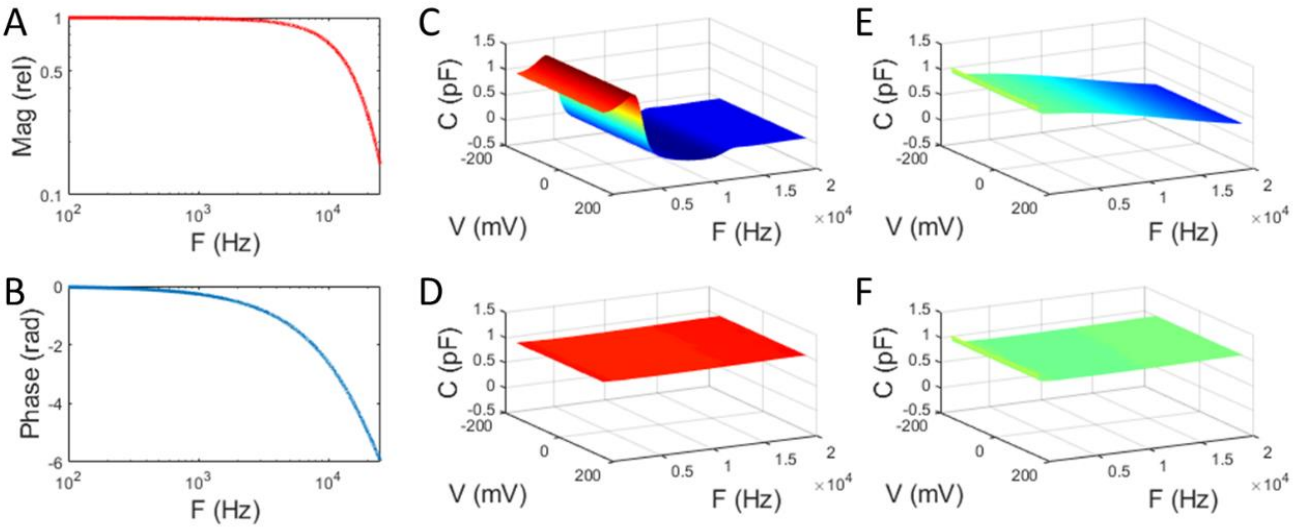

Figure S1 Requirement to correct for the frequency response of the patch clamp system prior to capacitance estimation, Related to Figure 1 and 2. A) Magnitude and B) phase of the system. Determination is detailed in the Methods. In C-D, a model electrical patch (R_s: 10 MΩ, R_m: 2GΩ, C_m: 1 pF) is used to confirm proper system performance. C,D) illustrate capacitance measures utilizing dual sine analysis and E,F) using single sine analysis as detailed in Methods. In C) and E) capacitance measures are not corrected for system frequency response. Responses are aberrant. In D) and F) corrections are made to the measured model patch admittance based on measured system admittance. Following corrections, capacitance measures are flat out to 20 kHz, across holding potentials of -160 to 160 mV.

References

Chessum, L., Matern, M. S., Kelly, M. C., Johnson, S. L., Ogawa, Y., Milon, B., McMurray, M., Driver, E. C., Parker, A., Song, Y., Codner, G., Esapa, C. T., Prescott, J., Trent, G., Wells, S., Dragich, A. K., Frolenkov, G. I., Kelley, M. W., Marcotti, W., Brown, S. D. M., Elkon, R., Bowl, M. R. & Hertzano, R. 2018. Helios is a key transcriptional regulator of outer hair cell maturation. *Nature*, 563(7733)**,** pp 696-700.

Dallos, P., Evans, B. N. & Hallworth, R. 1991. Nature of the motor element in electrokinetic shape changes of cochlear outer hair cells. *Nature*, 350(6314)**,** pp 155-157.

Duret, G., Pereira, F. A. & Raphael, R. M. 2017. Diflunisal inhibits prestin by chloride-dependent mechanism. *PLoS One,* 12(8)**,** pp e0183046.

Gillis, K. D. 1995. Techniques for Membrane Capacitance Measurements. *In:* Sakmann, B. & Neher, E. (eds.) *Single Channel Recording.* New York: Plenum Press.

Harasztosi, C. & Gummer, A. W. 2016. The chloride-channel blocker 9-anthracenecarboxylic acid reduces the nonlinear capacitance of prestin-associated charge movement. *Eur J Neurosci,* 43(8)**,** pp 1062-74.

Homma, K. & Dallos, P. 2011. Evidence that prestin has at least two voltage-dependent steps. *J.Biol.Chem.,* 286(3)**,** pp 2297-2307.

Huang, G. & Santos-Sacchi, J. 1993. Mapping the distribution of the outer hair cell motility voltage sensor by electrical amputation. *Biophys.J.,* 65(5)**,** pp 2228-2236.

Navarrete, E. G. & Santos-Sacchi, J. 2006. On the effect of prestin on the electrical breakdown of cell membranes. *Biophys.J.,* 90(3)**,** pp 967-974.

Pusch, M. & Neher, E. 1988. Rates of diffusional exchange between small cells and a measuring patch pipette. *Pflugers Arch.,* 411(2)**,** pp 204-211.

Santos-Sacchi, J. 2004. Determination of cell capacitance using the exact empirical solution of dY/dCm and its phase angle. *Biophys.J.,* 87(1)**,** pp 714-727.

Santos-Sacchi, J. 2018. High frequency measures of OHC nonlinear capacitance (NLC) and their significance: Why measures stray away from predictions. *AIP Conference Proceedings,* 1965(1)**,** pp 060004-1–060004-5.

Santos-Sacchi, J., Iwasa, K. H. & Tan, W. 2019. Outer hair cell electromotility is low-pass filtered relative to the molecular conformational changes that produce nonlinear capacitance. *J Gen Physiol,* jgp.201812280. doi: 10.1085/jgp.201812280(

Santos-Sacchi, J., Kakehata, S. & Takahashi, S. 1998. Effects of membrane potential on the voltage dependence of motility-related charge in outer hair cells of the guinea-pig. *J.Physiol,* 510 (Pt 1)(225-235.

Santos-Sacchi, J. & Navarrete, E. 2002. Voltage-dependent changes in specific membrane capacitance caused by prestin, the outer hair cell lateral membrane motor. *Pflugers Arch.,* 444(1-2)**,** pp 99-106.

Santos-Sacchi, J. & Song, L. 2014. Chloride and Salicylate Influence Prestin-dependent Specific Membrane Capacitance. *Journal of Biological Chemistry,* 289(15)**,** pp 10823-10830.

Santos-Sacchi, J. & Song, L. 2016. Chloride anions regulate kinetics but not voltage-sensor Qmax of the solute carrier SLC26a5. *Biophysical Journal,* 110(1-11.

Santos-Sacchi, J. & Tan, W. 2018. The Frequency Response of Outer Hair Cell Voltage-Dependent Motility Is Limited by Kinetics of Prestin. *J Neurosci,* 38(24)**,** pp 5495-5506.

Schnee, M. E., Santos-Sacchi, J., Castellano-Munoz, M., Kong, J.-H. & Ricci, A. J. 2011a. Calcium-Dependent Synaptic Vesicle Trafficking Underlies Indefatigable Release at the Hair Cell Afferent Fiber Synapse. *Neuron,* 70(2)**,** pp 326-338.

Schnee, M. E., Santos-Sacchi, J., Castellano-Munoz, M., Kong, J. H. & Ricci, A. J. 2011b. Tracking vesicle fusion from hair cell ribbon synapses using a high frequency, dual sine wave stimulus paradigm. *Communicative & Integrative Biology,* 4(6)**,** pp 785-787.